

Physics-Informed Neural Networks for Irregular Domain Mapping and Partial Differential Equations solving

Cuizhi Zhou, Kaien Zhu*

School of Physics, Nankai University, Tianjin 300071, People's Republic of China

*Email: zhukaien@nankai.edu.cn

June 15, 2025

Abstract

The solution of partial differential equations (PDES) on irregular domains has long been a subject of significant research interest. In this work, we present an approach utilizing physics-informed neural networks (PINNs) to achieve irregular-to-regular domain mapping. Thus we can use finite difference method and physics-informed convolutional neural networks to solve PDEs on rectangular grids instead of the original irregular boundary.

Structured grids on irregular domains are obtained by inverse mapping. We demonstrate PINN's versatile capability to produce customized structured grids tailored to diverse computational requirements, thereby significantly facilitating PDEs solving.

Keywords: Physics-Informed Neural Networks, Irregular Domains, Structured grids, Partial Differential Equations

1 Introduction

The numerical solution of partial differential equations (PDEs) on irregular domains has long been a challenging problem. Over the past few decades, the

primary numerical methods for addressing this issue have been the Finite Element Method (FEM)[1] and the Finite Volume Method (FVM) [2]. However, these methods impose stringent requirements on mesh quality. In 2019, M. Raissi et al. proposed the Physics-Informed Neural Network (PINN) model [3], which integrates the residuals of PDE governing equations, boundary conditions, and initial conditions into a multi-objective loss function. This approach enables the network to inherently satisfy physical laws during training. By eliminating the reliance on computational grids, PINN achieves direct modeling in continuous space, offering a novel solution for solving PDEs on irregular domains.

Despite its widespread application in PDE solving, PINN still suffers from low accuracy and excessively long training times when applied to irregular domains. Several improvements have been proposed to address these limitations. Complex geometries are embedded into a regular background grid, with the loss function distinguishing between interior and exterior domains to avoid explicit mesh generation [4, 5]. Distance functions are introduced into the loss function to weight residuals in the domain and on the boundary [6, 7, 8]. Dual-grid approaches [9] use one network satisfies the PDE and the other one handles boundary conditions . Domain mapping is presented in [10] where irregular domains are mapped to regular ones. We are interested in the domain mapping approach in [10] where elliptic coordinates are used for domain mapping and physics-informed convolutional neural networks (PICNN) is used for PDEs solving.

In this article we map irregular boundaries of PDEs to regular domains by PINN. We will show that PINN can generate customized grids. Structured meshes are obtained by inverse mapping. We can solve PDE on irregular domain with FEM or FVM on structured grid, or in a better way, we can solve mapped PDE on rectangular grids with finite difference method (FDM) or spectral method.

The paper is organized as follows: Section II Solve the PDE Equation in the Computational Space; Section III introduce grids generation techniques.

2 Solving PDEs in the Computational Space

Solving PDEs on irregular domains has long been a challenging problem. The primary numerical methods for addressing this issue have been the FEM[1] and the FVM [2]. Can we map irregular boundaries to rectangular boundaries

so that FDM or spectral method can work?

This section introduces a method to construct the mapping from irregular domains to regular domains using PINNs, thereby enabling efficient PDE solver such as FDM in the computational space (regular domain) . The rectangular space is referred to as the computational space, and the original space is called the physical space.

2.1 Domain mapping and PINN architecture

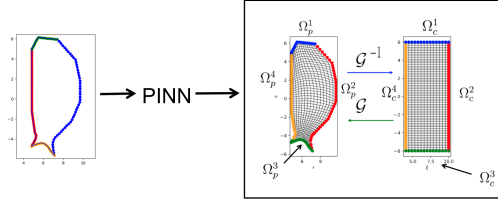


Fig. 1. The PINN mapping approach.

We follow the notation system in reference [10]. Grids are obtained by PINN method. The key point is to find the regular-to-irregular domain mapping $\mathcal{G} : \Omega_p \rightarrow \Omega_c$ in Fig. 1 with which structured meshes are obtained,

$$\mathbf{x} = \mathcal{G}(\boldsymbol{\xi}), \quad \forall \boldsymbol{\xi} \in \partial\Omega_c^i, i = 1, \dots, 4, \quad (1)$$

$$\boldsymbol{\xi} = \mathcal{G}^{-1}(\mathbf{x}), \quad \forall \mathbf{x} \in \partial\Omega_p^i, i = 1, \dots, 4. \quad (2)$$

PINN employs a Multi - Layer Perceptron (MLP) architecture in this article. The input of this neural network consists of the coordinates (ξ, η) in the computational space, while its output is the coordinates (x, y) in the physical space.

The loss function of PINN is:

$$L = \omega_{eq} \cdot L_{eq} + \omega_{bd} \cdot L_{bd} + \omega_{jac} \cdot L_{jac}, \quad (3)$$

where

$$L_{eq} = \frac{1}{N_f} \sum_{i=1}^{N_f} ((\nabla^2 x)^2 + (\nabla^2 y)^2), \quad (4)$$

$$L_{bd} = \frac{1}{N_b} \sum_{i=1}^N (u_\theta(\xi, \eta) - (x_i, y_i))^2, \quad (5)$$

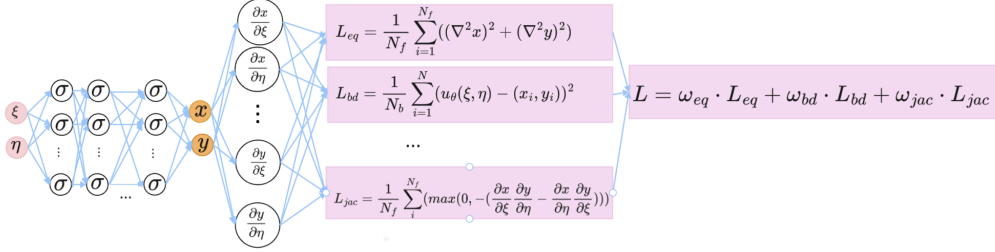


Fig. 2. Schematic diagram of the PINN model.

$$L_{jac} = \frac{1}{N_f} \sum_i^{N_f} (\max(0, -(\frac{\partial x}{\partial \xi} \frac{\partial y}{\partial \eta} - \frac{\partial x}{\partial \eta} \frac{\partial y}{\partial \xi}))), \quad (6)$$

$$\nabla^2 x = \frac{\partial^2 x}{\partial \xi^2} + \frac{\partial^2 x}{\partial \eta^2}, \quad \forall(\xi, \eta) \in \Omega_c, \quad (7)$$

$$\nabla^2 y = \frac{\partial^2 y}{\partial \xi^2} + \frac{\partial^2 y}{\partial \eta^2}, \quad \forall(\xi, \eta) \in \Omega_c. \quad (8)$$

The term L_{eq} means solving a diffusion equation in computational space which is different from [10] where a diffusion equation is solved in physical space. Laplacian-based regularization term of the loss function enforces local smoothness of the grid distribution.

The boundary loss function is L_{bd} , where N_b denotes the total number of discretely sampled points on the boundary, u_θ represents the mapping function constructed by the neural network with parameters θ , and (x_i, y_i) corresponds to the precise coordinate values of the i -th sampling point on the boundary of the physical computational domain.

To ensure the generated grid cells maintain valid topological structures, this paper introduces a Jacobian determinant constraint as a key regularization term L_{jac} , whose core objective is to enforce the mathematical condition $\det(J) > 0$ for each grid cell's Jacobian matrix.

By conducting optimization training based on the above composite loss function L , grids with excellent characteristics can be obtained. Figure 3 illustrates some numerical results. The mesh generated by PINN approach has high quality standards.

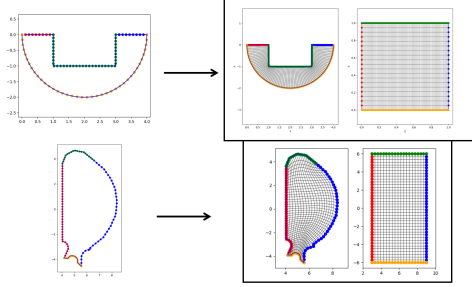


Fig. 3. PINN-generated meshes on irregular domains.

2.2 The technique to solve PDEs with irregular boundary

Irregular boundaries are mapped to rectangles and it is easy to get the grids of rectangles, which is shown in Fig 3. But how to use rectangular mesh to solve PDEs? The answer is to map equations of physical space to the ones of computational space since the map \mathcal{G} and \mathcal{G}^{-1} are established by PINN.

2.2.1 Transformation of equations to computational space

The transformation framework from physical space to computational space could be found in [11]. For ease of reference, the key points of the framework are presented here.

The transformation relationship of differential operators between the physical space and the computational space can be characterized by the following mathematical form:

$$\frac{\partial}{\partial x} = \frac{\partial}{\partial \xi} \frac{\partial \xi}{\partial x} + \frac{\partial}{\partial \eta} \frac{\partial \eta}{\partial x}, \quad (9)$$

$$\frac{\partial}{\partial y} = \frac{\partial}{\partial \xi} \frac{\partial \xi}{\partial y} + \frac{\partial}{\partial \eta} \frac{\partial \eta}{\partial y}. \quad (10)$$

The second-order derivatives can be derived:

$$\begin{aligned}
\frac{\partial^2}{\partial x^2} &= \frac{\partial}{\partial x} \left(\frac{\partial}{\partial x} \right) \\
&= \frac{\partial}{\partial x} \left(\frac{\partial \xi}{\partial x} \frac{\partial}{\partial \xi} + \frac{\partial \eta}{\partial x} \frac{\partial}{\partial \eta} \right) \\
&= \left(\frac{\partial \xi}{\partial x} \frac{\partial}{\partial \xi} + \frac{\partial \eta}{\partial x} \frac{\partial}{\partial \eta} \right) \left(\frac{\partial \xi}{\partial x} \frac{\partial}{\partial \xi} + \frac{\partial \eta}{\partial x} \frac{\partial}{\partial \eta} \right) \\
&= \left(\frac{\partial \xi}{\partial x} \right)^2 \frac{\partial^2}{\partial \xi^2} + 2 \frac{\partial \xi}{\partial x} \frac{\partial \eta}{\partial x} \frac{\partial^2}{\partial \xi \partial \eta} \\
&\quad + \left(\frac{\partial \eta}{\partial x} \right)^2 \frac{\partial^2}{\partial \eta^2} + \frac{\partial^2 \xi}{\partial x^2} \frac{\partial}{\partial \xi} + \frac{\partial^2 \eta}{\partial x^2} \frac{\partial}{\partial \eta},
\end{aligned} \tag{11}$$

$$\begin{aligned}
\frac{\partial^2}{\partial y^2} &= \frac{\partial}{\partial y} \left(\frac{\partial}{\partial y} \right) \\
&= \frac{\partial}{\partial y} \left(\frac{\partial \xi}{\partial y} \frac{\partial}{\partial \xi} + \frac{\partial \eta}{\partial y} \frac{\partial}{\partial \eta} \right) \\
&= \left(\frac{\partial \xi}{\partial y} \frac{\partial}{\partial \xi} + \frac{\partial \eta}{\partial y} \frac{\partial}{\partial \eta} \right) \left(\frac{\partial \xi}{\partial y} \frac{\partial}{\partial \xi} + \frac{\partial \eta}{\partial y} \frac{\partial}{\partial \eta} \right) \\
&= \left(\frac{\partial \xi}{\partial y} \right)^2 \frac{\partial^2}{\partial \xi^2} + 2 \frac{\partial \xi}{\partial y} \frac{\partial \eta}{\partial y} \frac{\partial^2}{\partial \xi \partial \eta} \\
&\quad + \left(\frac{\partial \eta}{\partial y} \right)^2 \frac{\partial^2}{\partial \eta^2} + \frac{\partial^2 \xi}{\partial y^2} \frac{\partial}{\partial \xi} + \frac{\partial^2 \eta}{\partial y^2} \frac{\partial}{\partial \eta}.
\end{aligned} \tag{12}$$

Laplace operator is

$$\nabla^2 T = \frac{1}{|J|} \left(\frac{\partial}{\partial \xi} \left(|J| \frac{\partial T}{\partial \xi} \right) + \frac{\partial}{\partial \eta} \left(|J| \frac{\partial T}{\partial \eta} \right) \right) \tag{13}$$

where J is the Jacobian matrix

$$J = \begin{bmatrix} \frac{\partial x}{\partial \xi} & \frac{\partial x}{\partial \eta} \\ \frac{\partial y}{\partial \xi} & \frac{\partial y}{\partial \eta} \end{bmatrix}. \tag{14}$$

2.2.2 FDM on computational domain

Take heat conduction equation with irregular boundary as an example. The boundary is shown in Fig. 4. The equation is

$$\nabla^2 T = \frac{\partial^2 T}{\partial x^2} + \frac{\partial^2 T}{\partial y^2} = 0, \quad (\mathbf{x}, \mathbf{y}) \in \Omega_p \quad (15)$$

$$T((\mathbf{x}, \mathbf{y})) = 0, \quad (\mathbf{x}, \mathbf{y}) \in \partial\Omega_{p, \text{up}} \quad (16)$$

$$T((\mathbf{x}, \mathbf{y})) = 1, \quad (\mathbf{x}, \mathbf{y}) \in \partial\Omega_{p, \text{left}}, \Omega_{p, \text{right}}, \Omega_{p, \text{down}} \quad (17)$$

where T is the temperature field of 2D domain. In the computational space, we need to solve the following equation:

$$\nabla^2 T = \frac{1}{|J|} \left(\frac{\partial}{\partial \xi} \left(|J| \frac{\partial T}{\partial \xi} \right) + \frac{\partial}{\partial \eta} \left(|J| \frac{\partial T}{\partial \eta} \right) \right) = 0, \quad (\mathbf{x}, \mathbf{y}) \in \Omega_c \quad (18)$$

$$T((\xi, \eta)) = 0, \quad (\xi, \eta) \in \partial\Omega_{c, \text{up}} \quad (19)$$

$$T((\xi, \eta)) = 1, \quad (\xi, \eta) \in \partial\Omega_{c, \text{left}}, \Omega_{c, \text{right}}, \Omega_{c, \text{down}} \quad (20)$$

FDM are used to solve the above equation and the data are mapped back to physical domain. This approach works quite satisfactory and the the results are presented in Fig. 4. The benchmark is also presented in Fig. 4 where FVM is used to solve the equation in OpenFOAM software.

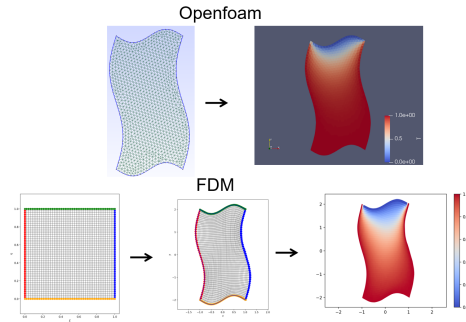


Fig. 4. Temperature distribution by OpenFOAM and FDM.

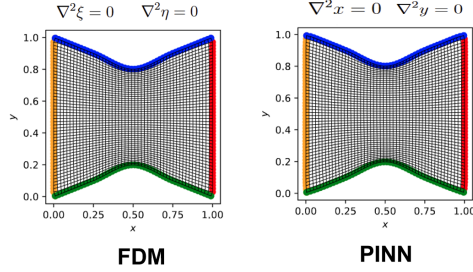


Fig. 5. Comparison between our PINN-generated mesh and FDM-generated mesh of [10]

2.3 Solve equation using PICNN

After the grids are established, there is another way to solve PDEs in computational domain where neural networks are used. In fact, physics-informed convolutional neural networks (PICNN) is such a technique [10].

Since convolutional neural network (CNN) only can handle regular geometries with image-like format, Gao et al. applied elliptic coordinate mapping to enable coordinate transforms between the irregular physical domain and regular computational domain [10], that is, they choose first to map

$$\frac{\partial^2 \xi}{\partial x^2} + \frac{\partial^2 \xi}{\partial y^2} = 0, \quad (21)$$

$$\frac{\partial^2 \eta}{\partial x^2} + \frac{\partial^2 \eta}{\partial y^2} = 0, \quad (22)$$

to computational domain and then to solve the mapped equations by traditional FDM algorithm.

Our approach in this article is to solve elliptic equation by PINN in computational domain directly, that is, Eq. 7 and Eq. 8. The equations are simpler and the PINN way is more flexible about which will be presented later.

Figure 5 presents the meshes generated by our PINN approach and FDM approach of [10]. Both methods produce high-quality meshes.

The steady Navier-Stokes equations for two-dimensional incompressible

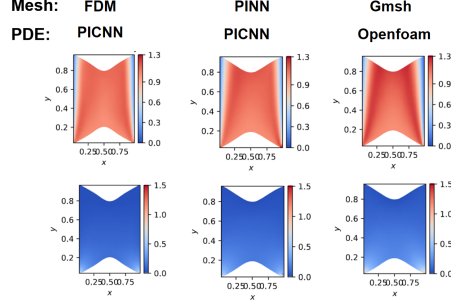


Fig. 6. Navier-Stokes equations solved by: (left) PICNN on FDM-generated grids; (middle) PICNN on PINN-generated grids; (right) OpenFOAM’s solution results of FVM.

fluid problems is

$$\begin{cases} \frac{\partial u}{\partial x} + \frac{\partial v}{\partial y} = 0 \\ \frac{\partial u}{\partial t} + u \frac{\partial u}{\partial x} + v \frac{\partial u}{\partial y} = -\frac{1}{\rho} \frac{\partial p}{\partial x} + \nu \left(\frac{\partial^2 u}{\partial x^2} + \frac{\partial^2 u}{\partial y^2} \right) \\ \frac{\partial v}{\partial t} + u \frac{\partial v}{\partial x} + v \frac{\partial v}{\partial y} = -\frac{1}{\rho} \frac{\partial p}{\partial y} + \nu \left(\frac{\partial^2 v}{\partial x^2} + \frac{\partial^2 v}{\partial y^2} \right) \end{cases} \quad (23)$$

where u and v represent the components of the velocity in the x and y directions respectively, p represents the pressure field, ρ is the density of the fluid, and ν is the kinematic viscosity coefficient.

Figure 6 displays the numerical solutions of the Navier-Stokes equations, where left column shows results obtained using PICNN on FDM-generated meshes (method of [10]), middle column presents solutions computed with PICNN on PINN-generated meshes (our approach), and right column provides reference solutions from OpenFOAM’s FVM. The comparative results demonstrate that the PICNN on PINN-generated meshes is a creditable approach for PDEs with irregular boundaries.

3 Grid generation techniques

In regions such as boundary layers, shock waves, chemical reaction interfaces, and fluid vortices, the spatial gradients of solution functions are extremely large, meaning that physical quantities change sharply over short distances. Therefore, we need to divide grids densely in such regions. Meanwhile, when the computational domain contains structures such as sharp corners or small holes, it is also necessary to divide grids densely.

Traditional body-fitted coordinate methods typically need to construct and solve sophisticated high-order partial differential equations (e.g., harmonic mapping equations, Winslow equations) to achieve specific grid characteristics. In this article we will show that PINN-based grid mapping approach is versatile for such situations by mathematically formulating requirements as loss functions.

Different requirements, such as boundary conformity, orthogonality, cell size distribution, etc., could be easily added into the loss function. This framework provides two major advantages: (1) eliminating the dual challenges of equation formulation and numerical solution in conventional methods, and (2) simultaneously handling geometric complexity and physical constraints.

3.1 Basic Smooth Grid

Smooth grids are the primary consideration in grid generation. Equation (4) is corresponded for this purpose. The preceding grids are obtained in this way. Figure 7 is another example for this basic grid-generation skill.

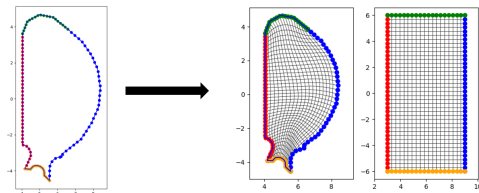


Fig. 7. Mesh generation for a tokamak's section.

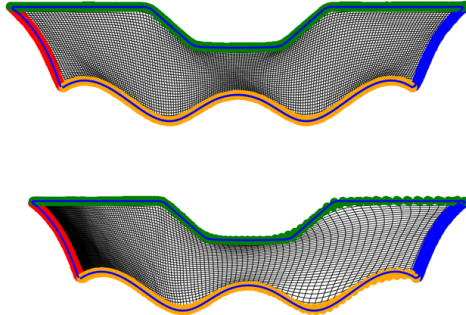


Fig. 8. Normal boundary layer (upper) vs. denser boundary layer (lower).

3.2 Denser boundary layer grids

Normal basic grids are generated where the boundaries are sampled evenly. Take the green boundary line of the upper figure of Fig. 8 for example. Let $t_k (k = 0, 1, \dots, N - 1)$ be evenly sampled points of $[0, 1]$ and L be the total length of the green line. Let s_k denotes the arc length of the natural coordinate system. Then

$$s_k = Lt_k \quad (24)$$

is the sampling points of green boundary line. The same procedure is applied to the orange boundary line and we get the grids shown in the upper figure of Fig. 8.

In practical applications of computational grids, some boundary regions often require higher mesh density to enhance calculation accuracy. To address this requirement, this study employs a exponential-function-based non-uniform sampling strategy that mathematically achieves gradient mesh refinement. The formula,

$$s_k = L \cdot \frac{e^{\alpha t_k} - 1}{e^\alpha - 1}, \quad (25)$$

gives out denser boundary layer grids, which is shown in the lower figure of Fig. 8. The parameter α controls the density of grids.

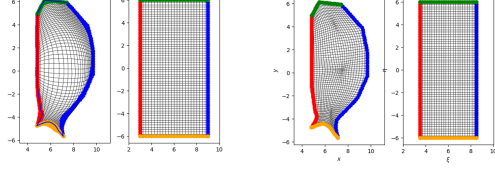


Fig. 9. Sparser and denser grids around specific points.

3.3 Sparser and denser grids around some points

We now present PINN-based grid generation method for sparser and denser grids around specific points. Figure 9 demonstrates these effects where the grids become sparser and denser at the regions around some points.

In the problem of grid generation, a mathematical framework for achieving the densification/sparsification of specific regions by adjusting the smooth term of the loss function can be constructed as follows:

$$L_{eq} = \frac{1}{N_f} \sum_{i=1}^{N_f} ((\nabla^2 x - P(\xi, \eta))^2 + (\nabla^2 y - Q(\xi, \eta))^2), \quad \forall (\xi, \eta) \in \Omega_c \quad (26)$$

where

$$\nabla^2 x = \frac{\partial^2 x}{\partial \xi^2} + \frac{\partial^2 x}{\partial \eta^2}, \quad (27)$$

$$\nabla^2 y = \frac{\partial^2 y}{\partial \xi^2} + \frac{\partial^2 y}{\partial \eta^2}, \quad (28)$$

and the expressions of $P(\xi, \eta)$ and $Q(\xi, \eta)$ are

$$P = \alpha \cdot \frac{\xi - \xi_0}{|\xi - \xi_0|} \cdot e^{-\beta[(\xi - \xi_0)^2 + (\eta - \eta_0)^2]}, \quad (29)$$

$$Q = \gamma \cdot \frac{\eta - \eta_0}{|\eta - \eta_0|} \cdot e^{-\beta[(\xi - \xi_0)^2 + (\eta - \eta_0)^2]}, \quad (30)$$

and (ξ_0, η_0) is the coordinate of the densified (sparsified) point in the computational space. By changing the signs of the functions $P(\xi, \eta)$ and $Q(\xi, \eta)$, the conversion function between sparsification and densification can be achieved. The parameters, α, β and γ are parameters that control the degree of distortions.

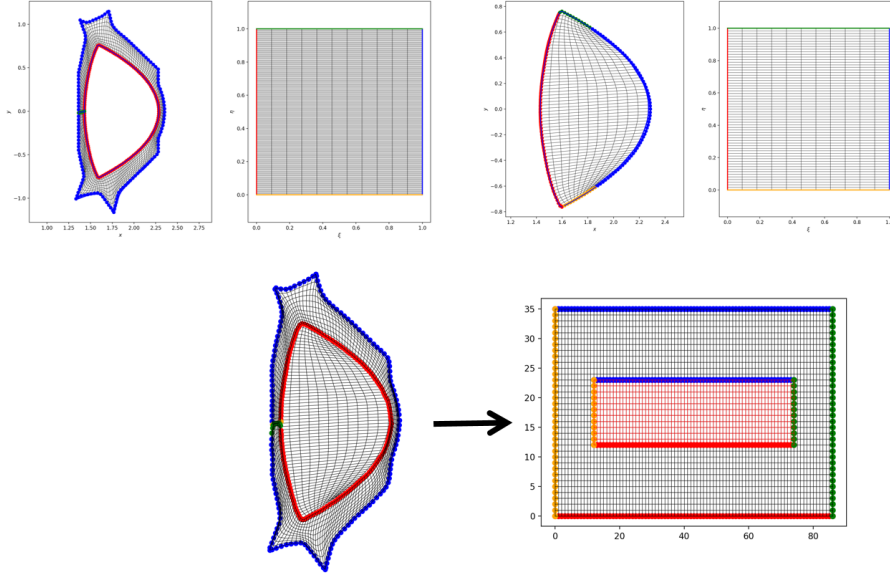


Fig. 10. Grid merging

3.4 Mesh merging

When solving physical problems, if different types of grids need to be generated for the interior and exterior of a device, PINN can be used to generate the structured grids separately, followed by grid merging process. In this way, the originally complex physical problem can be transformed into a computational task on two adjacent rectangular regions, thereby effectively reducing the computational complexity and improving the computational efficiency and accuracy.

As shown in Fig. 10, meshes can be merged to a unified one. The method of mesh merging is straightforward by taking the common sampling boundary points in physical space and by surrounding the rectangular grids of external region around the grids of internal region in computational space. PDEs can be solved on the irregular external region and the internal region separately, or they can be solved on the unified region. This method is more favorable for occasions where physical equations are different in different regions.

4 Conclusion

In this paper, the method of PINN is used to automatically generate structured grids and obtain the mapping relationship between irregular domains and regular domains, so that physical problems in irregular domains can be transformed and solved in rectangular domains. According to the characteristics of PINN, adding a loss function to the loss term can generate grids that meet special requirements. The grids generated by PINN can be used not only for traditional methods of solving PDE equations, such as FDM and the spectral method, but also for the AI based method, such as PICNN.

References

- [1] C. Astuto, D. Boffi, G. Russo, U. Zerbini, A nodal ghost method based on variational formulation and regular square grid for elliptic problems on arbitrary domains in two space dimensions, arXiv preprint arXiv:2402.04048 (2024).
- [2] S. Höllbacher, G. Wittum, Rotational test spaces for a fully-implicit fvm and fem for the dns of fluid-particle interaction, *Journal of Computational Physics* 393 (2019) 186–213. doi:<https://doi.org/10.1016/j.jcp.2019.05.004>.
- [3] M. Raissi, P. Perdikaris, G. Karniadakis, Physics-informed neural networks: A deep learning framework for solving forward and inverse problems involving nonlinear partial differential equations, *Journal of Computational Physics* 378 (2019) 686–707.
- [4] B. Khara, E. Herron, A. Balu, D. Gamdha, C.-H. Yang, K. Saurabh, A. Jignasu, Z. Jiang, S. Sarkar, C. Hegde, B. Ganapathysubramanian, A. Krishnamurthy, Neural pde solvers for irregular domains, *Computer-Aided Design* 172 (2024) 103709.
- [5] C. S. Peskin, The immersed boundary method, *Acta Numerica* 11 (2002) 479–517. doi:[10.1017/S0962492902000077](https://doi.org/10.1017/S0962492902000077).
- [6] N. Sukumar, A. Srivastava, Exact imposition of boundary conditions with distance functions in physics-informed deep neural networks, *Com-*

- puter Methods in Applied Mechanics and Engineering 389 (2022) 114333.
- [7] K. S. McFall, J. R. Mahan, Artificial neural network method for solution of boundary value problems with exact satisfaction of arbitrary boundary conditions, IEEE Transactions on Neural Networks 20 (8) (2009) 1221 – 1233. doi:[10.1109/TNN.2009.2020735](https://doi.org/10.1109/TNN.2009.2020735).
- [8] H. Sheng, C. Yang, Pfn: A penalty-free neural network method for solving a class of second-order boundary-value problems on complex geometries, Journal of Computational Physics 428 (2021) 110085. doi:<https://doi.org/10.1016/j.jcp.2020.110085>.
- [9] L. Lu, P. Jin, G. Pang, Z. Zhang, G. E. Karniadakis, Learning nonlinear operators via DeepONet based on the universal approximation theorem of operators, Nature Machine Intelligence 3 (3) (2021) 218–229.
- [10] H. Gao, L. Sun, J.-X. Wang, Phygeonet: Physics-informed geometry-adaptive convolutional neural networks for solving parameterized steady-state pdes on irregular domain, Journal of Computational Physics 428 (2021) 110079.
- [11] J. D. Anderson, Computational Fluid Dynamics :The Basic with Applications, McGraw-Hill Press, 1995.